AIAA JOURNAL
Vol. 42, No. 3, March 2004

Numerical Investigation of Shock-Reflection Phenomena in Overexpanded Supersonic Jets

A. Hadjadj*
Institut National des Sciences Appliquées, Saint Etienne du Rouvray 76801, France
and
A. N. Kudryavtsev† and M. S. Ivanov‡
Institute of Theoretical and Applied Mechanics, 630090, Novosibirsk, Russia

The transition from regular to Mach reflection in a supersonic planar jet operating under overexpanded conditions has been studied numerically. First, inviscid computations are performed by the solution of Euler equations. The results demonstrate that a hysteresis phenomenon is observed as the jet/ambient pressure ratio decreases and increases, causing a change in the angle of incidence of the nozzle-lip shock and, as a consequence, the transition from regular to Mach reflection and back. The angles of forward and backward transitions are close to the theoretical detachment and von Neumann criteria, respectively. Furthermore, turbulent computations (by the use of an improved two-equation model) are conducted to investigate the transition in a more realistic situation. The computations confirm the existence of the hysteresis and give the transition angles in very good agreement with both the theoretical criteria and the results of inviscid simulations. It appears that turbulence production is mainly concentrated in thin shear layers developing along the jet boundary, as well as the Mach stem slip streams, whereas the jet-core near field is characterized by a predominantly inviscid shock-cell structure. These observations justify the inviscid simulations when shock-wave reflection in the near field of supersonic jets is studied.

Nomenclature

c	=	speed of sound
d	=	dilatation
$\tilde{E}$	=	total energy per unit mass
$h/2$	=	jet half-width
k	=	turbulent kinetic energy
L_x, L_y	=	sizes of computational domain
M	=	Mach number
P	=	static pressure
P_k	=	production of kinetic energy
Pr	=	Prandtl number
$\tilde{q}$	=	heat flux
s	=	Mach stem height
T	=	temperature
t	=	time
u_i	=	velocity component in the x_i direction
α	=	shock-wave angle
γ	=	ratio of specific heats
ε	=	dissipation rate
θ	=	flow deflection angle
μ	=	viscosity
ρ	=	density
$\tilde{\tau}_{ij}$	=	viscous and turbulent stresses

Subscripts

a	=	ambient conditions
r	=	reservoir conditions
t	=	turbulent values

Superscripts

$\bar{}$	=	Reynolds-averaged quantities
$\tilde{}$	=	Favre-averaged quantities
$''$	=	fluctuations of Favre-averaged quantities

Presented as Paper 2002-0977 at the 40th Aerospace Sciences Meeting, Reno, NV, 14 January 2002; received 1 April 2003; revision received 30 September 2003; accepted for publication 14 October 2003.

*Research Scientist, Laboratoire de Mécanique des Fluides Numérique, Institut National des Sciences Appliquées de Rouen.

†Senior Research Scientist, Computational Aerodynamics Laboratory, Institute of Theoretical and Applied Mechanics.

‡Professor and Head, Computational Aerodynamics Laboratory, Institute of Theoretical and Applied Mechanics. Associate Fellow AIAA.

Introduction

THE aerodynamic study of supersonic jets exhausting from convergent–divergent nozzles is one of the most challenging problems in space and aeronautical applications. Various physical phenomena involved in this fluid dynamics problem are directly linked to the performance of jet engines. Though off-design operations with either overexpanded or underexpanded exhaust flow induce performance losses, in many cases such regimes cannot be avoided. The imperfect matching between the ambient pressure and the exit-nozzle pressure leads to the formation of a complicated shock wave structure. The flow gradually adapts to the ambient conditions as it passes through the system of shock waves. For several decades,[1] numerous investigations of the structure of supersonic jets have been undertaken, but the subject is quite complicated and not yet clearly understood.

In recent years, important progress has been achieved in understanding fundamental aspects of shock/shock interactions with an emphasis on the transition between regular and Mach reflections. It was revealed, both numerically[2] and experimentally,[3] that such a transition is accompanied by a hysteresis. Namely, if the incidence angle of the shock wave varies, the transition from regular to Mach reflection and back is observed at different angles, as was earlier conjectured by Hornung et al.[4]

Some typical configurations where the transition between regular and Mach reflections is observed are shown in Fig. 1 for the incident shock (IS), the reflected shock (RS), the jet boundary (JB), the Mach stem (MS), the slipstream surface (SS), and the expansion fan (EF), respectively. The flow around two symmetrical wedges (Fig. 1a) has been used in most experimental studies on shock wave reflection transition in steady flows. The flow in a channel with a ramp (Fig. 1b) can be considered a prototype of flows in real supersonic inlets. For both of these flows, it is well documented now[5,6] that in numerical

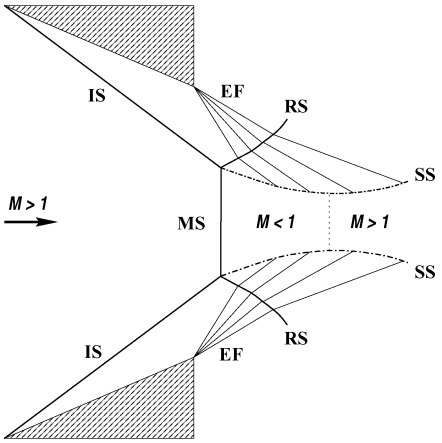

a) Flow between two wedges

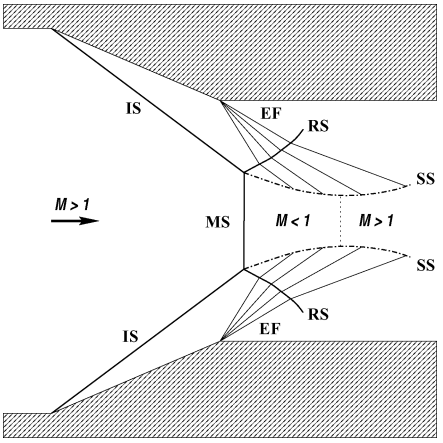

b) Flow in channel with ramp

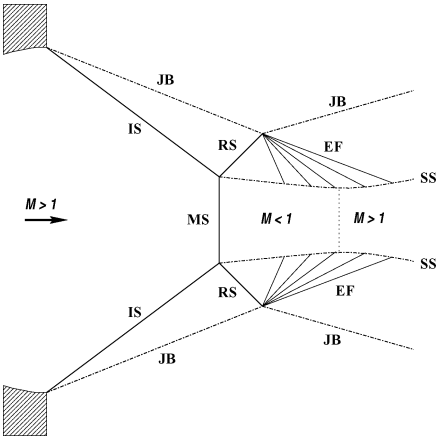

c) Overexpanded jet flow

Fig. 1 Three types of flows where the transition between RR and MR is observed.

simulations where, unlike wind-tunnel experiments, there are no freestream disturbances, the transition to MR occurs at the incident shock wave angle α equal to the so-called detachment angle α_d and the back transition, at α equal to the von Neumann angle α_N.

The angles α_d and α_N are the theoretical criteria deduced from the analysis of shock wave reflection using pressure-deflection diagrams.[7] Regular reflection (RR) is theoretically impossible above α_d, whereas MR is not possible below α_N. At high Mach numbers, these two angles bound an interval of the incident shock wave angles, the dual solution domain (Fig. 2), where both RR and MR can exist. Numerical experiments give clear evidence that the transition to MR occurs when, on an increase of the angle, the upper boundary of the domain is crossed, and the reverse transition is observed when, on a decrease of the angle α, the lower boundary is

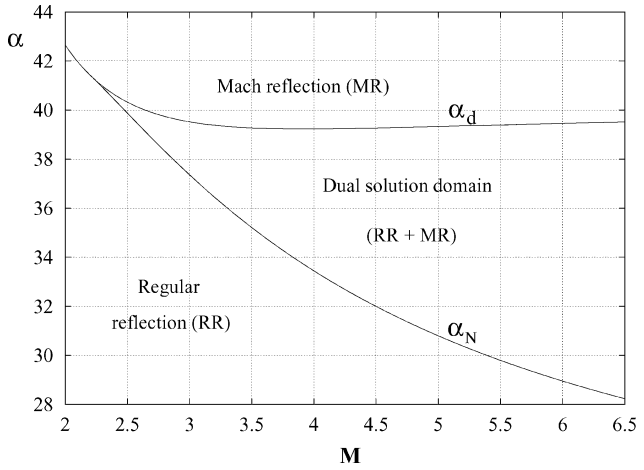

Fig. 2 Theoretical transition criteria; incident shock wave angles as function of Mach number.

reached. Thus, two different types of reflection can be obtained at the same angle within the dual solution domain, and the change in the shock wave configuration is accompanied by a hysteresis phenomenon.

Note that the situation with wind-tunnel observation of hysteresis is more complicated, given the influence of freestream disturbances, which are inevitably present in any experimental facility. Nevertheless, it is possible to obtain experimental values of the transition angles quite close to theoretical ones by the use of a low-noise wind tunnel.[8]

The shock wave reflection transition is also a salient feature in supersonic imperfectly expanded jets. The variation of the pressure ratio between the jet and ambient space changes the incidence angle of either the nozzle-lip shock (for overexpanded jets) or the barrel shock (for underexpanded jets). It can be assumed that the hysteresis phenomenon should also occur in such flows. The simplest geometrical configuration for this case is shown in Fig. 1c. For nozzles operating under highly overexpanded flow conditions, the shock generated at the edge of the nozzle is so strong that a RR from the centerline is not possible, and MR occurs. In Fig. 1c, where a typical MR is shown, a triple point appears somewhere along the straight IS. An RS and an MS, which is a strong shock, are initiated from the triple point along with an SS, which indicates the entropy discontinuity. Here, in contrast to an axisymmetric jet and a planar underexpanded jet, both the IS and the JB (before its interaction with the RS) are straight. Hence, direct comparisons with the theoretical criteria are possible. Experimental schlieren photographs[9] showing the evolution of the shock waves as a function of the reservoir/ambient pressure ratio P_r/P_a are given in Fig. 3, where both RR and MR are observed.

Note that there is some experimental[10,11] and numerical[12] evidence of the hysteresis phenomena in underexpanded axisymmetric jets. However, it is difficult to say if such investigations refer to the same type of hysteresis as in the case of planar jets.

The goal of the present paper is to investigate numerically the shock wave reflection transition in planar overexpanded jets to establish definitively whether the transition is accompanied by the hysteresis. First, the Euler simulations are carried out with a high-order weighted essentially nonoscillatory (WENO) scheme. Then, a second-order total variation diminishing (TVD) scheme is used to conduct Navier–Stokes computations with the k–ε turbulence model. It allows us to investigate a more realistic case of a high Reynolds number turbulent jet and to try to elucidate the impact of viscosity and turbulence on the shock wave reflection transition.

This paper is organized as follows: In the following section, the compressible Favre-averaged Navier–Stokes equations are briefly presented with the turbulence model that has been utilized. The numerical techniques are also given in this section. Results of both inviscid and turbulent computations are presented and discussed in the next section, leading to the conclusions given at the end.

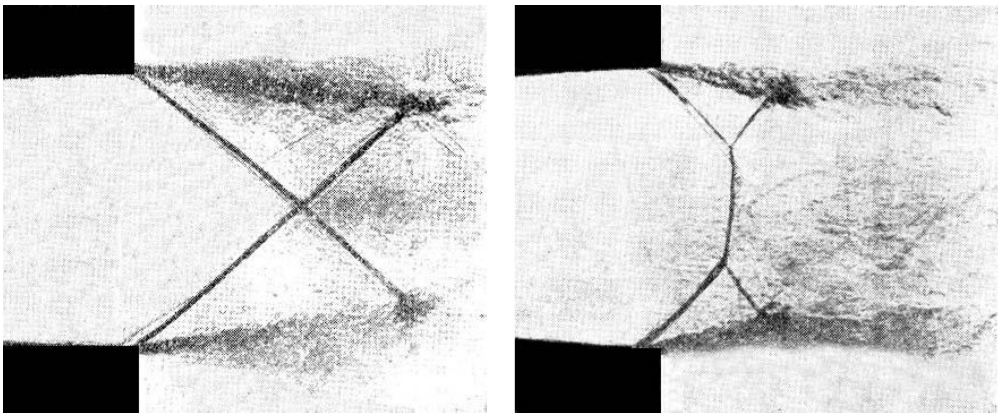

a) b)

Fig. 3 Experimental schlieren photographs showing a) RR for $P_r/P_a = 3.84$ and b) MR for $P_r/P_a = 3.54$; photographs from Ref. 9.

Theoretical Formulation, Turbulence Modeling, and Numerics

Governing Equations

Let $\bar{f}$ denote a common, Reynolds-averaged, value of a quantity f; whereas $\tilde{f}$ is a mass-averaged (Favre) value, $\tilde{f} = \overline{\rho f}/\bar{\rho}$; and $f'' = f - \tilde{f}$. Then, the Favre-averaged Navier–Stokes equations for a compressible turbulent fluid flow can be written as follows:

$$\frac{\partial}{\partial t}\bar{\rho} + \frac{\partial}{\partial x_j}\bar{\rho}\tilde{u}_j = 0 \tag{1}$$

$$\frac{\partial}{\partial t}\bar{\rho}\tilde{u}_i + \frac{\partial}{\partial x_j}(\bar{\rho}\tilde{u}_i\tilde{u}_j + \bar{P}\,\delta_{ij} - \tilde{\tau}_{ij}) = 0 \tag{2}$$

$$\frac{\partial}{\partial t}\bar{\rho}\tilde{E} + \frac{\partial}{\partial x_j}[(\bar{\rho}\tilde{E} + \bar{P})\tilde{u}_j - \tilde{\tau}_{ij}\tilde{u}_i - \tilde{q}_j] = 0 \tag{3}$$

The tensor $\tilde{\tau}_{ij}$ is a sum of viscous and turbulent stresses

$$\tilde{\tau}_{ij} = (\tilde{\mu} + \mu_t)\left(\frac{\partial \tilde{u}_i}{\partial x_j} + \frac{\partial \tilde{u}_j}{\partial x_i} - \frac{2}{3}\,\delta_{ij}\frac{\partial \tilde{u}_l}{\partial x_l}\right) - \frac{2}{3}\bar{\rho}k\,\delta_{ij} \tag{4}$$

and the turbulent heat flux is

$$\tilde{q}_j = \gamma\left(\frac{\tilde{\mu}}{Pr} + \frac{\mu_t}{Pr_t}\right)\frac{\partial\,\tilde{e}}{\partial x_j} + \frac{\mu_t}{\sigma_k}\frac{\partial k}{\partial x_j} \tag{5}$$

The set of flow equations is closed by the use of the perfect gas law to relate pressure to density and internal energy

$$\bar{P} = (\gamma - 1)\bar{\rho}\,\tilde{e} = (\gamma - 1)\bar{\rho}\left[\tilde{E} - \tfrac{1}{2}(\widetilde{u_i u_i} + \widetilde{u_i'' u_i''})\right] \tag{6}$$

where γ is the specific heat ratio, taken as 1.4.

The molecular dynamic viscosity is expressed as a function of temperature by the Sutherland law

$$\frac{\tilde{\mu}}{\mu_0} = \sqrt{\frac{\tilde{T}}{T_0}}\,\frac{1 + 110.4/T_0}{1 + 110.4/\tilde{T}}$$

where $T_0 = 273.15$ K and $\mu_0 = 1.711 \cdot 10^{-5}$ kg/(m · s), $\tilde{e}$ is the internal energy, and $\tilde{E}$ is the total energy per unit mass.

In Euler simulations, $\tilde{\tau}_{ij}$ and $\tilde{q}_j$ are put to zero. In turbulent computations, the two-equation k–ε model is used to evaluate the turbulent viscosity μ_t via the turbulent kinetic energy k and dissipation ε. Details of the turbulence model used are given in the next subsection.

Turbulence Modeling

The k–ε model is the most widely known and extensively used two-equation eddy viscosity model. It was originally developed to improve the mixing-length model and to avoid the algebraic description of the turbulent length scale in complex flows.[13] Different versions of this model can be found in the literature.[14] The model gives reasonably good results for free shear layer flows. For wall-bounded flows, the model provides good agreement with experimental results for zero and low mean pressure gradients, but is less accurate for high adverse pressure gradients.[14]

When turbulent freejet flows are computed, the use of the standard k–ε model is an appropriate way to predict correctly the mean and the turbulent flow parameters. However, for high-speed flows, it is important to include compressible dissipation and pressure-dilatation effects in the two-equation turbulence models as suggested by Sarkar,[15] Sarkar et al.,[16] and Vandromme.[17]

In this study, we used an improved version of the k–ε turbulence model to account for compressibility effects.[15,16,18]

Turbulence energy transport equation:

$$\underbrace{\frac{\mathrm{D}(\bar{\rho}\,k)}{\mathrm{D}t}}_{\text{Transport}} = \underbrace{\frac{\partial}{\partial x_j}\left[\left(\mu + \frac{\mu_t}{\sigma_k}\right)\frac{\partial k}{\partial x_j}\right]}_{\text{Diffusion}} + \underbrace{P_k}_{\text{Production}} - \underbrace{\bar{\rho}\,(\varepsilon_s + \varepsilon_c)}_{\text{Destruction}} + \underbrace{\overline{p''d''}}_{\text{Pressure dilatation}} \tag{7}$$

where k is the turbulent kinetic energy per unit mass, defined as $k = \frac{1}{2}\widetilde{u_i'' u_i''} = \frac{1}{2}[\widetilde{u_1''^2} + \widetilde{u_2''^2} + \widetilde{u_3''^2}]$, and ε_c and $\overline{p''d''}$ represent the contributions due to compressible dissipation and pressure dilatation, respectively.

Energy dissipation transport equation:

$$\frac{\mathrm{D}(\bar{\rho}\,\varepsilon_s)}{\mathrm{D}t} = \frac{\partial}{\partial x_j}\left[\left(\mu + \frac{\mu_t}{\sigma_\varepsilon}\right)\frac{\partial \varepsilon_s}{\partial x_j}\right] + C_{\varepsilon 1}\frac{\varepsilon_s}{k}P_k - C_{\varepsilon 2}\,\bar{\rho}\,\frac{\varepsilon_s^2}{k} \tag{8}$$

in which the turbulent viscosity is expressed as

$$\mu_t = C_\mu \bar{\rho}(k^2/\varepsilon)$$

and $P_k = -\bar{\rho}\widetilde{u_i'' u_j''}(\partial \tilde{u}_i/\partial x_j)$ is the exact turbulent kinetic energy production. Here, $-\bar{\rho}\widetilde{u_i'' u_j''}$ is the Reynolds stress, defined as follows:

$$-\bar{\rho}\widetilde{u_i'' u_j''} = \mu_t\left(\frac{\partial \tilde{u}_i}{\partial x_j} + \frac{\partial \tilde{u}_j}{\partial x_i} - \frac{2}{3}\,\delta_{ij}\frac{\partial \tilde{u}_l}{\partial x_l}\right) - \frac{2}{3}\,\delta_{ij}\bar{\rho}k$$

The model constants are given by $C_\mu = 0.09$, $C_{\varepsilon 1} = 1.44$, $C_{\varepsilon 2} = 1.92$, $\sigma_k = 1.0$, $Pr = 0.72$, $Pr_t = 0.9$, and $\sigma_\varepsilon = 1.3$.

Based on direct numerical simulation of isotropic turbulence and homogeneous shear flows, Sarkar et al.[16] proposed the following model for pressure dilatation:

$$\overline{p''d''} = -\alpha_2\,\bar{\rho}\,P_k\,M_t^2 + \alpha_3\,\bar{\rho}\,\varepsilon_s\,M_t^2$$

Here, $M_t = \sqrt{k}/c$ is the turbulent Mach number and c is the speed of sound.

The dissipation rate of turbulent kinetic energy contains two parts, the solenoidal (incompressible) and dilatational (compressible) parts, ε_s and ε_c, respectively,

$$\varepsilon = \varepsilon_s + \varepsilon_c$$

where ε_s is computed from the incompressible form of ε [Eq. (8)] and ε_c is assumed to be a function of ε_s and the turbulent Mach number M_t:

$$\varepsilon_c = \alpha_1 M_t^2 \varepsilon_s$$

Sarkar[16] recommends that $\alpha_1 = 0.5$, $\alpha_2 = 0.4$, and $\alpha_3 = 0.2$.

Numerical Techniques and Boundary Conditions

A fifth-order finite difference WENO scheme[19] was used to solve Euler equations. The WENO schemes are very appropriate for the problem under consideration because they have the property of robust shock capturing and provide high accuracy in the regions where the solution is smooth. The global Lax–Friedrichs splitting was applied when the numerical fluxes were calculated, and the third-order TVD Runge–Kutta scheme was used to advance the solution in time.

In turbulent computations, the governing equations for the mean flow and turbulence quantities were integrated with an explicit second-order finite volume scheme. For the convective terms, the upwind TVD scheme of Harten[20] with van Leer's limiter was used, and central-difference methods were employed for the diffusion terms of the momentum, energy, and turbulence equations. A second-order Runge–Kutta scheme was used for the time marching.

Numerical simulations with turbulence modeling are rather time consuming. The average computational time for each simulation was approximately 30 h CPU (global time) with 10 processors on a parallel computer (ORIGIN 2000). In all of the simulations, the Courant–Friedrichs–Lewy (CFL) number was fixed at 0.8. The freestream conditions were

$$M_a \simeq 0, \qquad P_a = 101322\,\text{Pa}, \qquad T_a = 300\,\text{K}$$

Low freestream values (nearly zero) of the turbulent kinetic energy k and the dissipation rate ε were fixed near the freestream at rest. These values were kept constant for all of the simulations. For turbulent free-shear flows, the $k-\varepsilon$ model showed no sensitivity to freestream turbulence.[21]

The boundary conditions are of different types. Because of the symmetry nature of the problem, only one-half of the jet is computed. Symmetry boundary conditions are applied along the axis of symmetry. Nonreflective boundary conditions with a fixed value of the static pressure[22] are used along the outer boundary corresponding to the external freestream. A part of the inlet of the computational domain coincides with the jet inlet, where uniform flow is assumed to exit from an idealized nozzle. At a very high Reynolds number, the boundary layer developing at the nozzle wall is very thin, and its influence on the mean core of the jet is very weak; therefore, uniform supersonic boundary conditions at $M_{\text{jet}} = 5$ can be prescribed at the nozzle exit. The rest of the inlet boundary is assumed to be a solid wall. For the turbulence transport equations, either zeroth-order extrapolation or freestream values are used for k and ε along the outer boundaries. If the flow is outgoing along the outer boundary, zeroth-order extrapolation is used. If there is flow entrainment, then freestream values are imposed along the outer boundaries. At the inflow, the nondimensional turbulent kinetic energy is defined as $K^* \equiv \sqrt{k}/U_{\text{jet}} \simeq 2\%$, where U_{jet} is the velocity of the jet. Once k is known, ε is obtained with the production-equals-dissipation hypothesis.

The size of the computational domain is $L_x = 2h$ in the streamwise direction and $L_y = h$ in the cross-streamwise direction, where h is the nozzle width. In inviscid simulations, the grid cell size is such that 100 cells are located across the nozzle half-width $h/2$. The turbulent computations employ 500×250 equally spaced points. Grid-independent results are obtained by the use of this mesh; the height of the Mach stem is used as a criterion for obtaining a grid-independent solution for $M_{\text{jet}} = 5$ and $\alpha = 42$ deg.

Results and Discussion

Inviscid Simulations

Shock–shock interaction is primarily an inviscid phenomenon, and the attempt to reproduce these interactions on the basis of the Euler equations seems to be natural. Results of inviscid simulations are given in Fig. 4, where the computed flowfields are presented

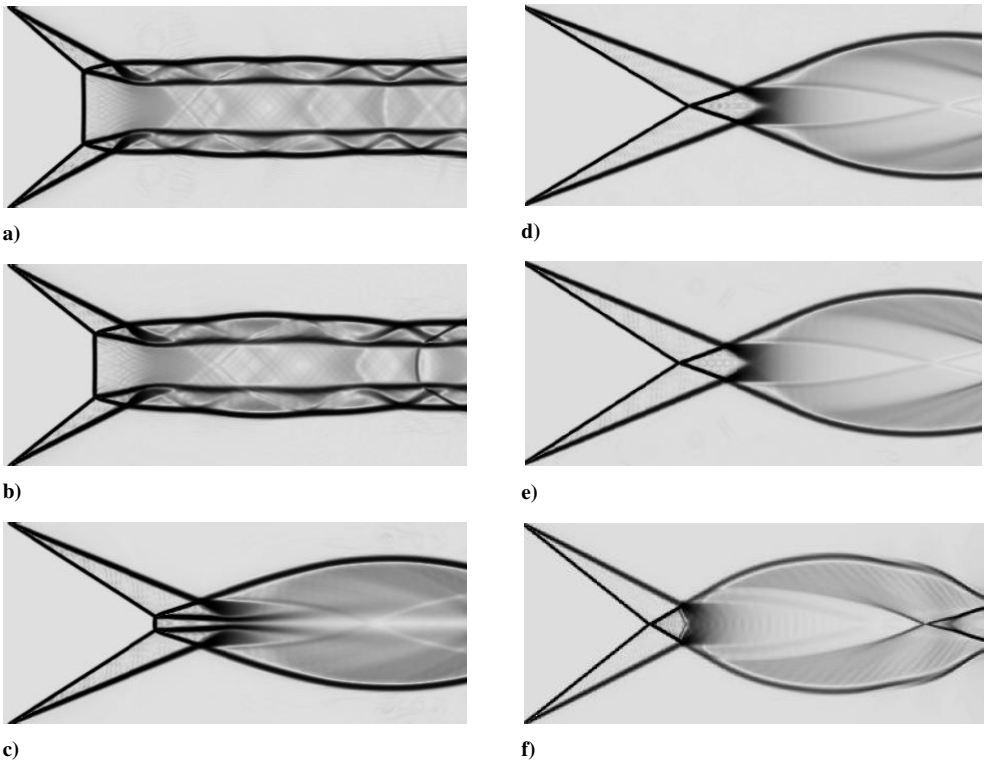

Fig. 4 Numerical schlieren pictures of overexpanded jet flow at $M_{\text{jet}} = 5$: a) $\alpha = 41$ deg, b) $\alpha = 39$ deg, c) $\alpha = 33$ deg, d) $\alpha = 31$ deg, e) $\alpha = 33$ deg, and f) $\alpha = 39$ deg.

as numerical schlieren images. This technique of visualization, proposed by Quirk,[23] portrays the absolute value of the density gradient with a nonlinear scale amplifying small gradients. The intensity of gray color is proportional to the quantity

$$\exp\left(-K\frac{|\nabla\rho|-|\nabla\rho|_{\min}}{|\nabla\rho|_{\max}-|\nabla\rho|_{\min}}\right)$$

where the minimum and maximum are calculated over all flowfields and K is a tunable parameter. ($K=15$ in the present paper.) Numerical schlieren images display very clearly gasdynamic discontinuities and, simultaneously, expose even weak density nonuniformities.

The computations were started for the jet/ambient pressure ratio P_{jet}/P_a corresponding to the incident shock angle $\alpha=41$ deg. It is noticeably higher than the detachment angle, which is $\alpha_d=39.3$ deg. Consequently, only MR is possible in this case. The ambient conditions in the entire computational domain were taken as the initial flowfield for this computation. After the complex transient process of startup of the jet flow, the flow began evolving to the steady state, and a converged solution was finally achieved (Fig. 4a). In each subsequent computation, the convergent flowfield of the preceding computation was used as initial data. The variation of jet pressure imposed as a boundary condition on the nozzle exit corresponded to a 2-deg change in the nozzle-lip shock angle. The MR was preserved when increasing P_{jet} until the value $\alpha=31$ deg was reached (Figs. 4c and 4d). This is in good agreement with the theoretically predicted von Neumann angle $\alpha_N=30.8$ deg. In numerical simulation, an earlier transition to regular reflection can be expected because it is impossible to resolve a very small MS whose height is comparable to the grid-cell size.

Afterward, the pressure ratio was decreased. The reflection remained regular over all of the dual solution domain, and the transition to MR occurred when the angle of incidence was changed from 39 to 41 deg (Figs. 4f and 4a). It again agrees with the theoretical detachment angle. Thus, an evident hysteresis phenomenon was observed: Within the dual solution domain, both regular and MR can be obtained, depending on the initial conditions of the computation. This hysteresis is very similar to that observed earlier in numerical simulations of the flow around two symmetrical wedges and the flow in a converging channel.

The computed flowfields show substantially different shock wave structures for RR and MR at the same value of P_{jet}/P_a. (Compare Figs. 4b and 4f.) In Fig. 5, the pressure distributions along the centerline for these two shock wave configurations are compared. Note that the pressure rise behind the reflection point of the nozzle-lip shock is significantly higher in the case of RR. It is in accordance with shock-polar analysis (Fig. 6), where the points RR and MR correspond to the states behind two incident and reflected oblique

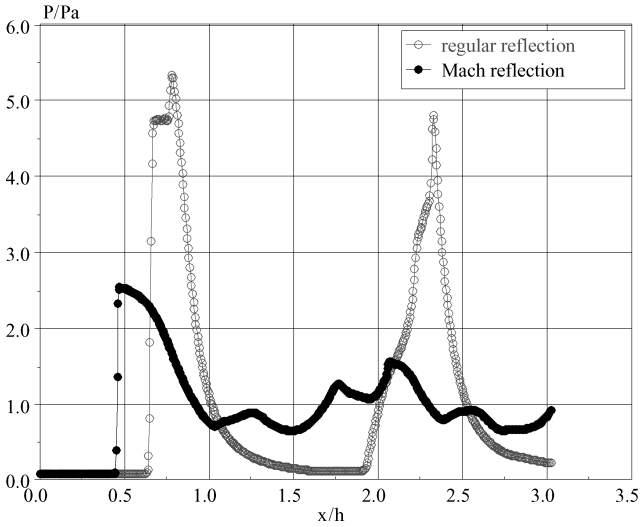

Fig. 5 Pressure distributions along the centerline for regular and Mach reflection at $\alpha=39$ deg.

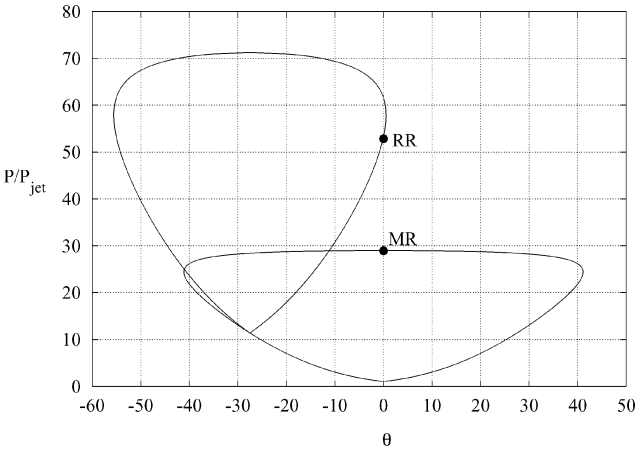

Fig. 6 Deflection angle: pressure diagram for $\alpha=39$ deg.

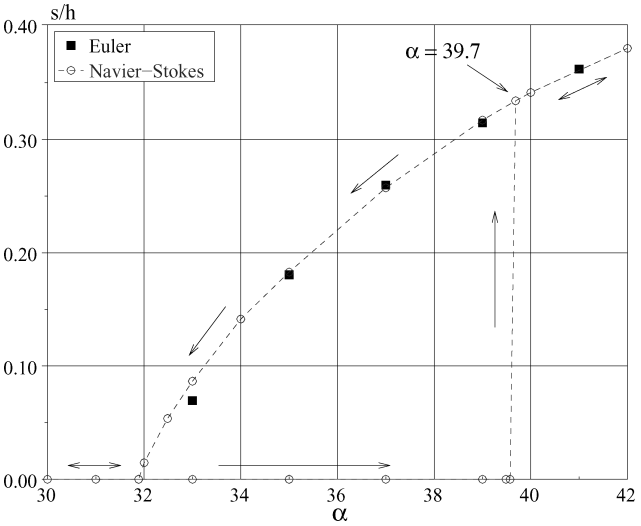

Fig. 7 Dependence of nondimensional Mach stem height *s/h* on the incident shock angle.

shock waves and behind the normal MS, respectively. In the case of RR, the jet boundary is strongly curved, and intensive compression waves are focused to the centerline, causing a secondary increase in pressure in addition to the primary peak at the reflection point. For MR, however, the only strong pressure rise is observed immediately behind the MS. Farther downstream, the pressure decreases as the flow accelerates again to supersonic velocities and later oscillates in a periodical system of compression and rarefaction waves within the jet core bounded by two SS emanating from the triple points.

Important quantities for practical applications are the position of the MS and its size. Therefore, several semi-analytical models were developed to predict these quantities for overexpanded jets.[24,25] Actually, the MS height is determined by the interaction between the EF and the SS originated from the triple point. The EF, which is generated as a result of the interaction of the RS wave with the JB, bends the SS, so that a virtual nozzle is formed. The relations between quantities in the entrance plane of the virtual nozzle (coinciding with the MS) and its throat, where the flow is sonic, control the position and the size of the MS. This mechanism, responsible for the existence of the steady MR configuration, is essentially the same as that clearly described in Ref. 26 for the case of reflection of a wedge-generated shock wave.

The Mach normalized stem heights, s/h, deduced from numerical results are presented in Fig. 7. Note a nonlinear behavior of s at angles close to α_N. It seems that the extrapolation of the curve should give a more accurate value for the angle of transition to regular reflection of about 32 deg. Also, a more accurate estimation of the transition angles will be made in the next section with the data from Navier–Stokes simulations.

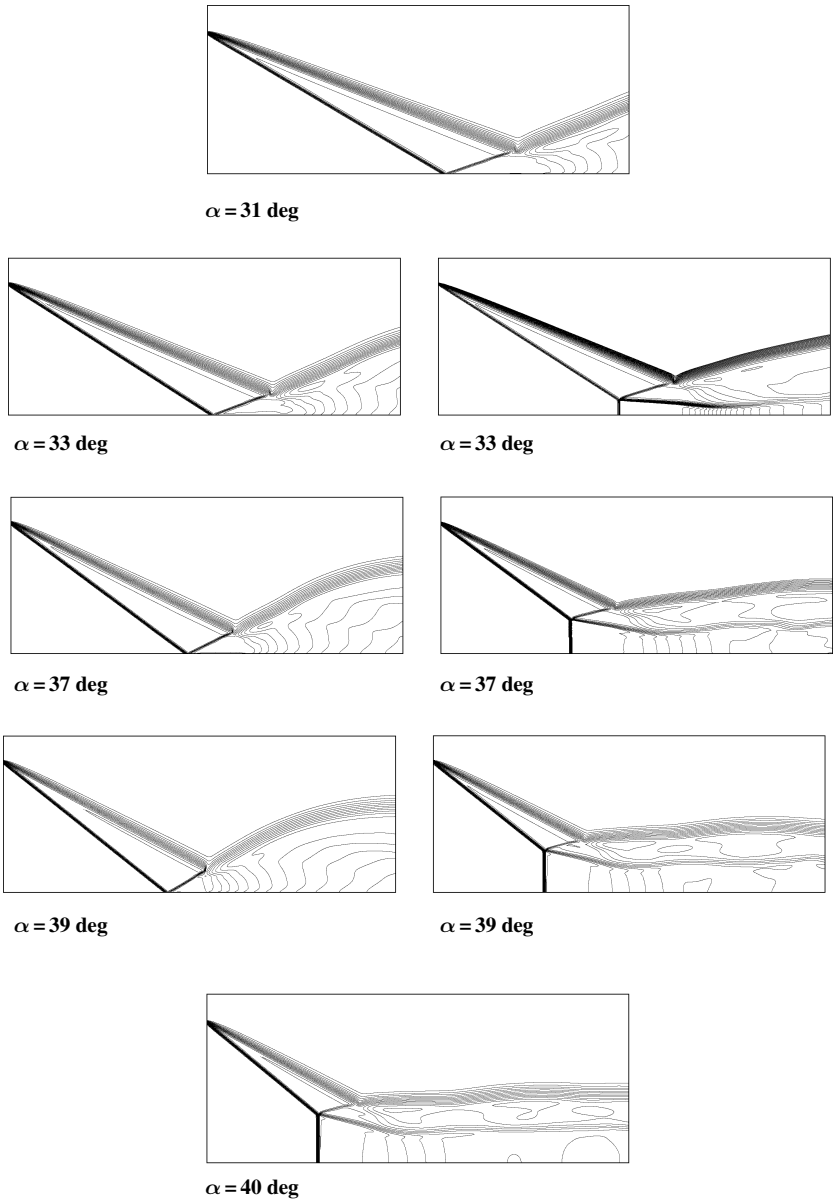

Fig. 8 Hysteresis phenomenon during the transition between regular and Mach configurations in a supersonic overexpanded turbulent jet; Mach number contours for $M_{\text{jet}} = 5$ and for different values of α.

Turbulent Computations

A series of turbulent jet computations at $M_{\text{jet}} = 5$ were carried out for a set of pressure ratios corresponding to incident shock wave angles α ranging from 31 to 42 deg, which covers the whole dual solution domain.

Figure 8 shows the evolution of the jet structure when the jet/ambient pressure ratio P_{jet}/P_a is increased and decreased. The computation was started from the case where only RR is possible ($\alpha = 31$ deg). After convergence, the pressure ratio was progressively decreased, step by step, down to a sudden transition to MR observed at $\alpha = 39.7$ deg. This angle is very close to the theoretical value of $\alpha = 39.3$ deg obtained with the detachment criterion. The back transition was observed when the shock wave angle was changed from $\alpha = 32$ to 31 deg. Note that, for $\alpha = 32$ deg, we still have MR with a small visible MS (Fig. 9). This angle slightly exceeds the value of $\alpha = 30.9$ deg theoretically predicted by the von Neumann criterion.

The dependence of the normalized MS heights, s/h, on the incident shock wave angle, α for $M_{\text{jet}} = 5$ is shown in Fig. 7. The hysteresis effect on increasing and decreasing the jet/ambient pressure ratio is evident. Note that the MS heights measured in the Navier–Stokes and Euler simulation are surprisingly close to each other.

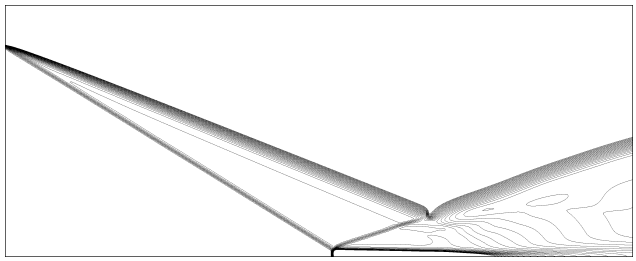

Fig. 9 Numerical calculation of the Mach number contours of Mach reflection wave configuration for $M_{\text{jet}} = 5$ and $\alpha = 32$ deg; note the existence of a small visible Mach stem with a normalized size of $s/h \simeq 0.015$.

The normalized turbulent kinetic energy, k/U_{jet}^2, flowfield is shown in Fig. 10 for both RR and MR configurations. For both cases, there is no turbulence in the central part of the jet (potential core). Turbulence production occurs essentially in the high-shear regions of the jet with additional compressibility effects. However, the jet-core near field is characterized by a predominantly inviscid shock-cell structure, where both turbulent and viscous effects are negligible. Because neither production nor amplification of

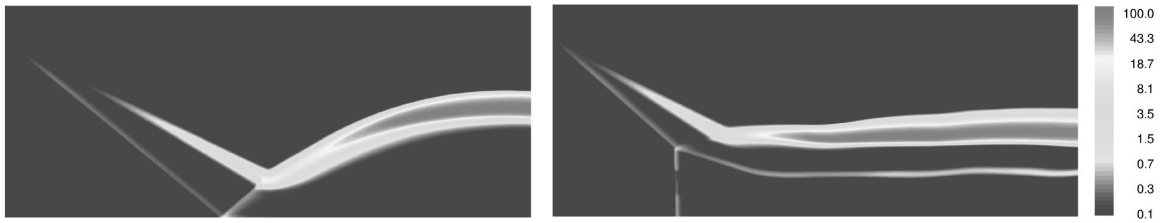

Fig. 10 Turbulent kinetic energy flowfield normalized by the square of centerline jet velocity U_{jet} in the case of a) regular reflection at $\alpha = 31$ deg and b) Mach reflection at $\alpha = 42$ deg.

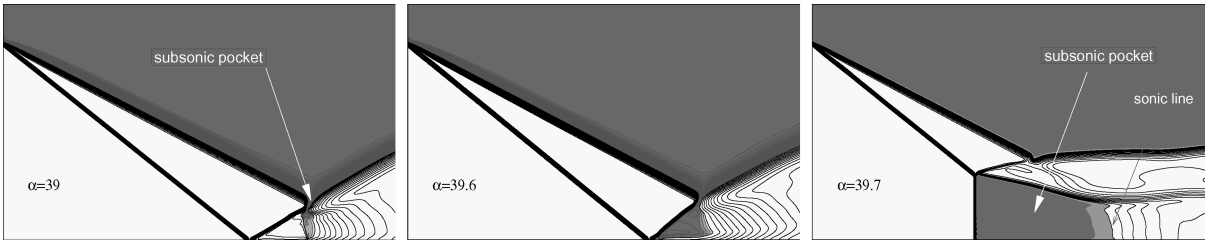

Fig. 11 Detailed numerical results for the flow Mach number contours of the turbulent jet and for three different values of the incident shock wave angle α at the beginning of the transition RR → MR.

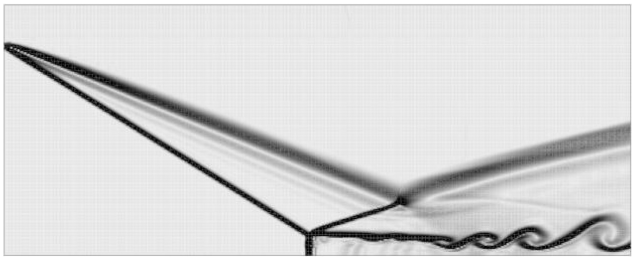

Fig. 12 Kelvin–Helmholtz instability along the slip surface emanating from the triple point at the transient process when changing the value of α from 35 to 33 deg (numerical schlieren image).

turbulence across shocks occur in this region, the contribution of Eqs. (7) and (8) to the total energy budget is nearly zero.

A detailed analysis of the flowfield during the RR → MR transition reveals the existence of a subsonic pocket downstream of the RS when α approaches the value of 39 deg. This phenomenon is shown in Fig. 11 for different values of α. Each photograph corresponds to a steady-state solution. In fact, when α is close to 39 deg, a subsonic pocket occurs just at the interaction between the RS and the JB. The size of this pocket grows progressively toward the jet symmetry line when α is increased and contaminates locally the flow downstream of the RS. The transition to MR occurs when the downstream RS flow becomes entirely subsonic.

Figure 12 illustrates a high-shear layer instability corresponding to the Kelvin–Helmholtz vortices emanating from the triple point. These vortices have a short lifetime and act essentially during the transient process. They completely disappear when the steady-state solution is reached. The possible influence of these vortices on the transition between RR and MR or on the stability of either Mach or regular configurations has yet to be studied and understood.

Finally, the possibility of experimental confirmation of the hysteresis phenomenon as described earlier is addressed. As is known,[5] the observation of the hysteresis for the two-wedge flow depends strongly on the level of disturbances in the wind tunnel used. A high level of disturbances can lead to an earlier transition to MR and even to a complete absence of the hysteresis phenomenon. It is difficult to predict a priori whether the overexpanded freejet is a more or less noisy flow and, consequently, more or less suitable for experiments on the hysteresis at the shock wave reflection transition. An additional problem can be that, at high Mach numbers, the nozzle-lip shock is rather strong and can induce a boundary-layer separation inside the nozzle that should destroy the gasdynamic scheme considered in this paper.

Conclusions

The shock wave reflection transition in an overexpanded supersonic jet at the Mach number $M_{\text{jet}} = 5$ has been numerically simulated. First, the Euler computations show that the transition from RR to MR and the back transition occur in agreement with the theoretical detachment and the von Neumann criteria, respectively. Thus, the dependence of the shock reflection type on initial conditions and the hysteresis phenomenon have been observed.

Furthermore, numerical investigations of the transition between RR and MR in steady turbulent overexpanded jets have been performed with the two-equation k–ε model modified to account for compressibility effects. Very good agreement of the computational results with the theoretical criteria of transitions, as well as with the results of the inviscid simulations has been found. Turbulence production was concentrated within the jet boundary layer and did not affect the jet-core flow substantially. As a result, the hysteresis effect was also observed when the jet/ambient pressure ratio was increased and decreased. The numerical study reveals that, when the jet pressure ratio is sufficiently low, subsonic conditions appear downstream of the RS for the RR configuration. To better understand this phenomenon, which probably triggers the transition from RR to MR, further analytical and numerical studies for solution of the problem of interaction between the RS and the JB should be undertaken. Also, further investigations should consider the effect on the shock wave configuration of the nozzle boundary layer and its possible separation.

Acknowledgments

Computational facilities were provided by the Institut du Développement et des Ressources en Informatique Scientifique-Centre National de la Recherche Scientifique, Paris, and the Centre de Ressources Informatiques de Haute Normandie, Rouen. The support of International Association for the Promotion of Co-Operation with Scientists from the New Independent States of the Former Soviet Union Grant 99-0785 is gratefully acknowledged. The Russian authors are also grateful to the Russian Foundation for Basic Research for support under Grant 03-01-00244.

References

[1]Ladenburg, R., Van Voorhis, C. C., and Winckler, J., "Interferometric Studies of Faster Than Sound Phenomena. Part II. Analysis of Supersonic Air Jets," *Physical Review*, Vol. 76, No. 5, 1949, pp. 662–677.

[2]Ivanov, M. S., Gimelshein, S. F., and Beylich, A. E., "Hysteresis Effect in Stationary Reflection of Shock Waves," *Physics of Fluids*, Vol. 7, No. 4, 1995, pp. 685–687.

[3]Chpoun, A., Passerel, D., Li, H., and Ben-Dor, G., "Reconsideration of Oblique Shock Wave Reflection in Steady Flows. Part I. Experimental Investigation," *Journal of Fluid Mechanics*, Vol. 301, 1995, pp. 19–35.

[4]Hornung, H. G., Oertel, H., and Sandeman, R. J., "Transition to Mach Reflexion of Shock Waves in Steady and Pseudo-Steady Flow with and Without Relaxation," *Journal of Fluid Mechanics*, Vol. 90, 1979, pp. 541–560.

[5]Ivanov, M. S., Vandromme, D., Fomin, V. M., Kudryavtsev, A. N., Hadjadj, A., and Khotyanovsky, D. V., "Transition Between Regular and Mach Reflection of Shock Waves: New Numerical and Experimental Results," *Shock Waves*, Vol. 11, No. 3, 2001, pp. 199–207.

[6]Ben-Dor, G., Ivanov, M. S., Vasilev, E. I., and Elperin, T., "Hysteresis Processes in the Regular Reflection ↔ Mach Reflection Transition in Steady Flows," *Progress in Aerospace Sciences*, Vol. 38, 2002, pp. 347–387.

[7]Ben-Dor, G., *Shock Wave Reflection Phenomena*, Springer-Verlag, New York, 1991, pp. 1–37.

[8]Ivanov, M. S., Kudryavtsev, A. N., Khotyanovsky, D. V., Nikiforov, S. B., and Pavlov, A. A., "Experiments on Shock Wave Reflection Transition and Hysteresis in Low-Noise Wind Tunnel," *Physics of Fluids*, Vol. 15, No. 6, 2003, pp. 1807–1810.

[9]Carafoli, E., *High-Speed Aerodynamics*, Editura Tehnica, Bucharest, Romania, 1956, pp. 442, 443.

[10]Teshima, K., "Structure of Supersonic Free-Jets Issuing from a Rectangular Orifice," *Progress in Astronautics and Aeronautics*, Vol. 158, 1994, pp. 375–380.

[11]Welsh, F. P., "Electron Beam Fluorescence Measurements of Shock Reflection Hysteresis in an Under-Expanded Supersonic Jet," *Proceedings of the 21st International Symposium on Shock Waves*, edited by A. F. P. Houwing, Vol. 2, Panther Publishing, Fyshwick, Australia, 1997, pp. 863–868.

[12]Gribben, B. J., Badcock, K. J., and Richards, B. E., "Numerical Study of Shock-Reflection Hysteresis in an Underexpanded Jet," *AIAA Journal*, Vol. 38, No. 2, 2000, pp. 275–283.

[13]Jones, W. P., and Launder, B. E., "The Prediction of Laminarization with a Two-Equation Model of Turbulence," *International Journal of Heat and Mass Transfer*, Vol. 15, 1972, pp. 301–314.

[14]Patel, C., Rodi, W., and Scheuerer, G., "Turbulence Models for Near-Wall and Low Reynolds Number Flows: A Review," *AIAA Journal*, Vol. 23, No. 9, 1985, pp. 1308–1319.

[15]Sarkar, S., "Modeling the Pressure–Dilatation Correlation," ICASE, Rept. 91-42, Hampton, VA, May 1991.

[16]Sarkar, S., Erlebacher, G., and Hussaini, M. Y., "Compressible Homogeneous Shear: Simulation and Modeling," *Proceedings of the 8th Symposium on Turbulent Shear Flows*, edited by F. Durst, B. E. Launder, and R. Friedrich, Springer-Verlag, Berlin, 1992, pp. 249–267.

[17]Vandromme, D., "Contribution à la Modélisation et à la Prédiction d'Écoulements Turbulents à Masse Volumique Variable," Ph.D. Dissertation, Departement de Mecanique, Univ. des Sciences et Techniques de Lille, Lille, France, Sept. 1983.

[18]Lakshmanan, B., and Abdol-Hamid, K. S., "Investigation of Supersonic Jet Plumes Using an Improved Two-Equation Turbulence Model," *Journal of Propulsion and Power*, Vol. 10, No. 5, 1994, pp. 736–741.

[19]Jiang, G.-S., and Shu, C.-W., "Efficient Implementation of Weighted ENO Schemes," *Journal of Computational Physics*, Vol. 126, No. 1, 1996, pp. 202–228.

[20]Harten, A., "High Resolution Scheme for the Computation of Weak Solutions of Hyperbolic Conservation Laws," *Journal of Computational Physics*, Vol. 49, 1983, pp. 357–393.

[21]Hadjadj, A., Vandromme, D., and De Chantérac, L., "Computations of Compressible Turbulent Shear Flows with Multiple-Time-Scale Models," *Proceedings of the 11th Symposium on Turbulent Shear Flows*, edited by F. Durst, B. E. Launder, F. W. Schmidt, and J. H. Whitelaw, Vol. 3, Institut National Polytechnique de Grenoble, Grenoble, France, 1997, pp. 32–38.

[22]Rudy, D., and Strikwerda, J., "A Non-Reflecting Outflow Boundary Condition for Subsonic Navier–Stokes Calculations," *Journal of Computational Physics*, Vol. 36, No. 1, 1980, pp. 55–70.

[23]Quirk, J. J., "A Contribution to the Great Riemann Solver Debate," *International Journal of Numerical Methods in Fluids*, Vol. 18, No. 6, 1994, pp. 555–574.

[24]Chow, W. L., and Chang, I. L., "Mach Reflection Associated with Overexpanded Nozzle Freejet Flows," *AIAA Journal*, Vol. 13, No. 6, 1975, pp. 762–766.

[25]Li, H., and Ben-Dor, G., "Mach Reflection Wave Configuration in Two-Dimensional Supersonic Jets of Overexpanded Nozzles," *AIAA Journal*, Vol. 36, No. 3, 1997, pp. 488–491.

[26]Hornung, H. G., and Robinson, M. L., "Transition from Regular to Mach Reflection of Shock Waves. Part 2. The Steady-Flow Criterion," *Journal of Fluid Mechanics*, Vol. 123, 1982, pp. 155–164.

M. Sichel
Associate Editor